EGU General Assembly 2020
Vienna | Austria | 3–8 May 2020

University of Tehran

A Quantitative Assessment of the Impact of Increase in CO_2 Concentration on Baroclinic Instability

Mahshid Kaviani, Farhang Ahmadi-Givi, Ali. R. Mohebalhojeh, and Daniel Yazgi
(Institute of Geophysics, University of Tehran, Iran)

Email: mahshid.kaviani@ut.ac.ir

CO_2 Radiative Properties

Carbon dioxide:
- Linear structure
- No permanent electric dipole moment
- Oscillating dipole moment

Transmission spectrum of CO_2

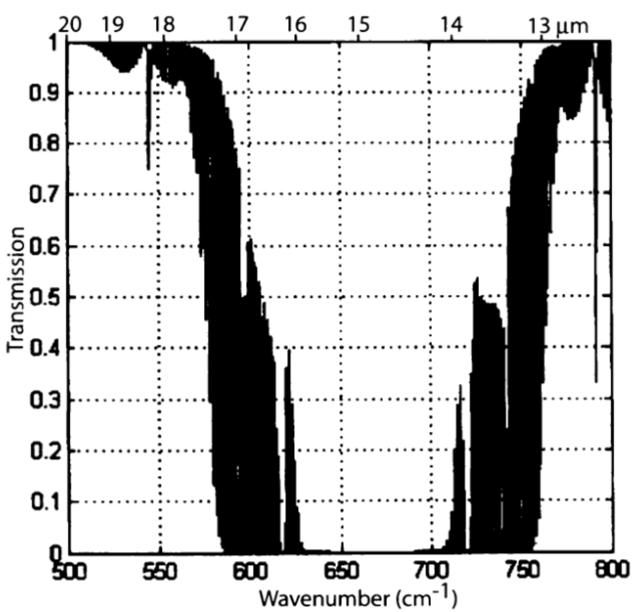

Petty (2006), Fig. 9.12

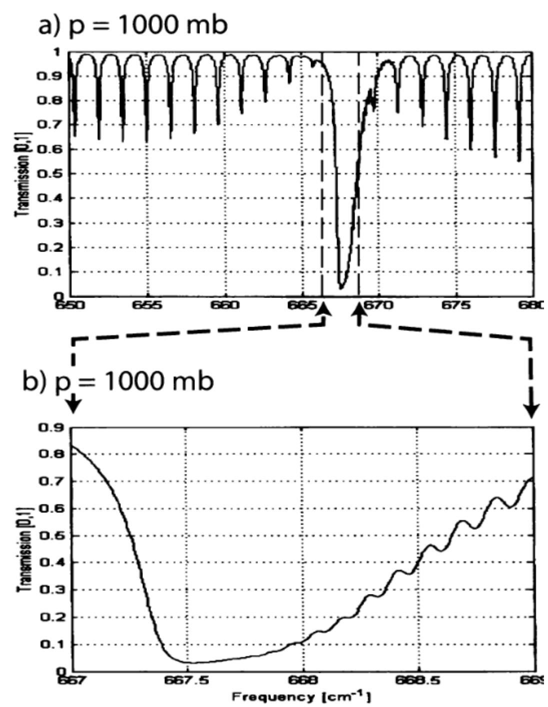

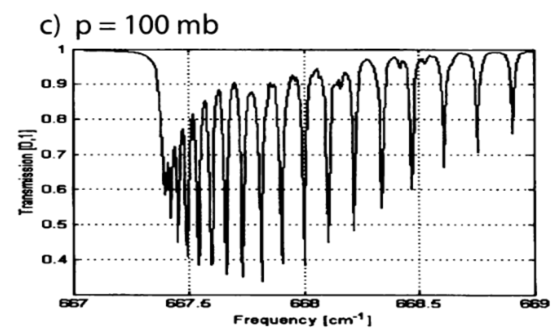

Petty (2006), Fig. 9.13

Radiative-Dynamical Core Interaction

GCMs structure

Physical packages

Dynamical core

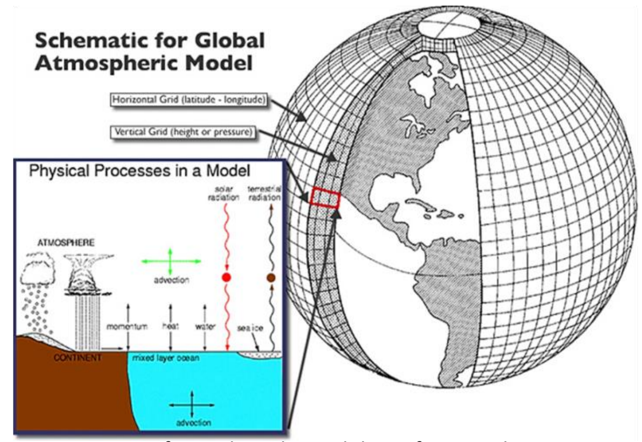

Source: Center for Multiscale Modeling of Atmospheric Processes

Input data:

- Temprature
- Pressure
- Active gasses
- Optical properties of clouds & aerosols

Radiative transfer scheme

Output data:

- Radiative fluxes
- Heating (cooling) rate

Radiative transfer model

Thermodynamic energy equation

Dynamical core

CO_2 Radiative Impacts on Baroclinic Instability

The same initial conditions + Different CO_2 concentrations

Radiative transfer model → **Baroclinic instability test case** → **Dynamical core**

Aim: Assessing the impact of increase in CO_2 concentration on baroclinic instability

Initial Conditions for Five Experiments

CO_2

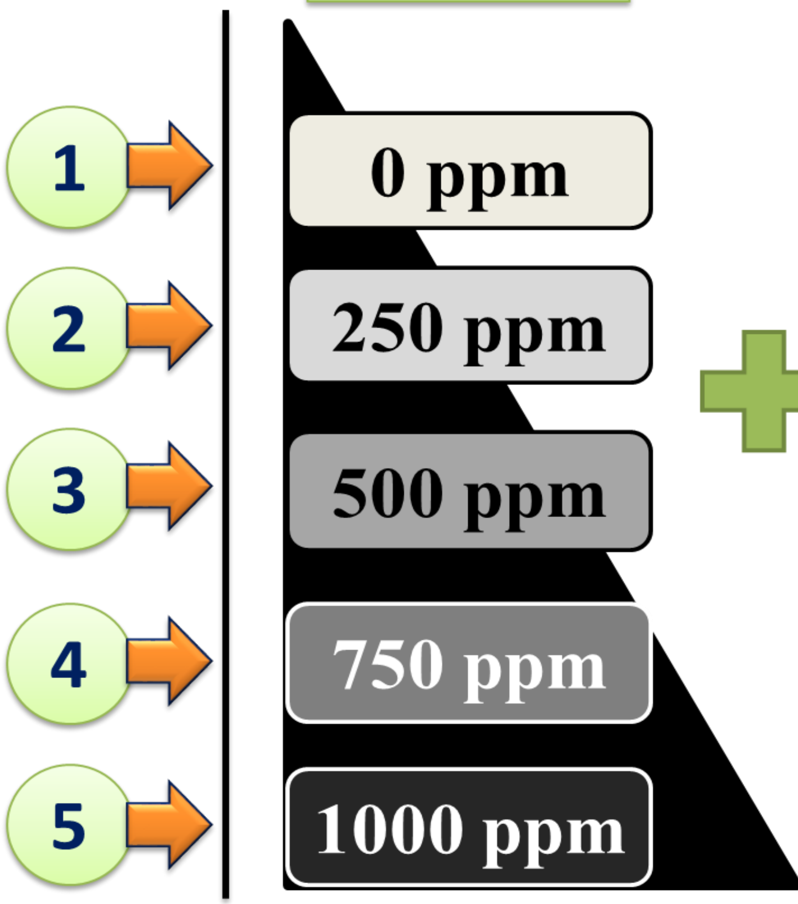

$P \;, \theta$

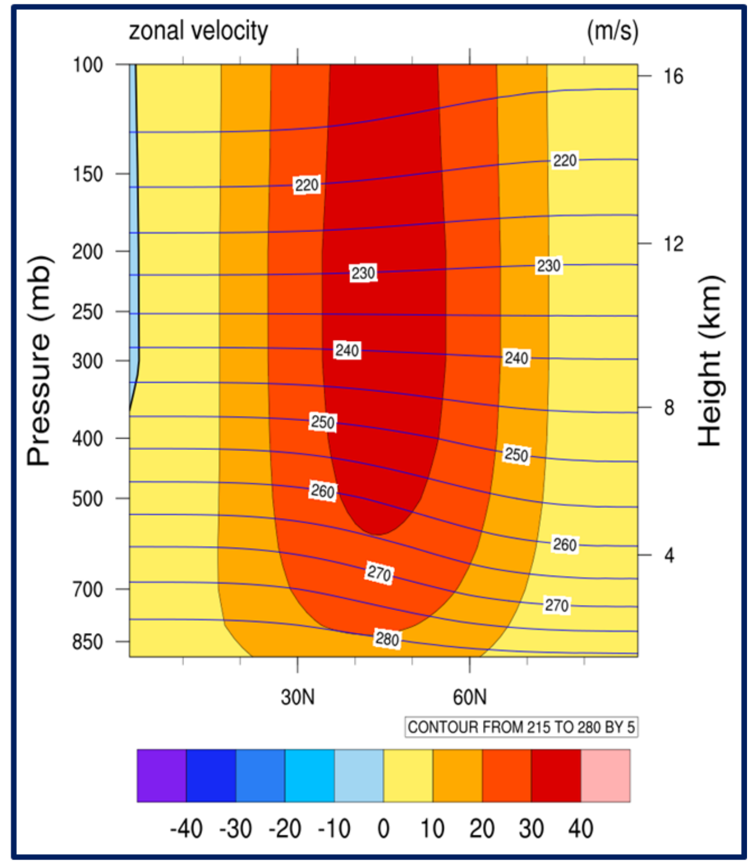

Start on 1 January 2009-12UTC , Integration time: 20 days

Radiative Transfer Scheme

aer
Atmospheric and Environmental Research

ECMWF NCAR LMD METEO FRANCE

Setting:

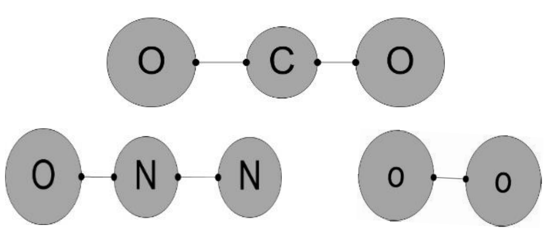

No aerosol & clear sky

No PBL, surface albedo set to 0.3

University of Tehran

Performance of Baroclinic Instability

Jablonowski & Williamson baroclinic instability test case (2006)

1

Defining the initial condition

Innovation:

The Newtonian relaxation ⇨ **Radiative transfer scheme**

$$\frac{\partial T}{\partial t} = -k(T - T_a)$$

$$\frac{\partial T}{\partial t} = -\frac{1}{\rho C_P}\frac{\Delta F(z)}{\Delta z}$$

2

Triggering baroclinic instability by adding a perturbation to an analytically defined zonal mean jet in a steady state

Dynamical Core

DCASL Based on potential vorticity

CASL
(Mohebalhojeh and Dritschel, 2004)

DCASL
(Mohebalhojeh and Dritschel, 2007 & 2009)

DCASL
(Mohebalhojeh et al, 2016)

Vertical coordinate: $\xi = F(\sigma, \theta)$

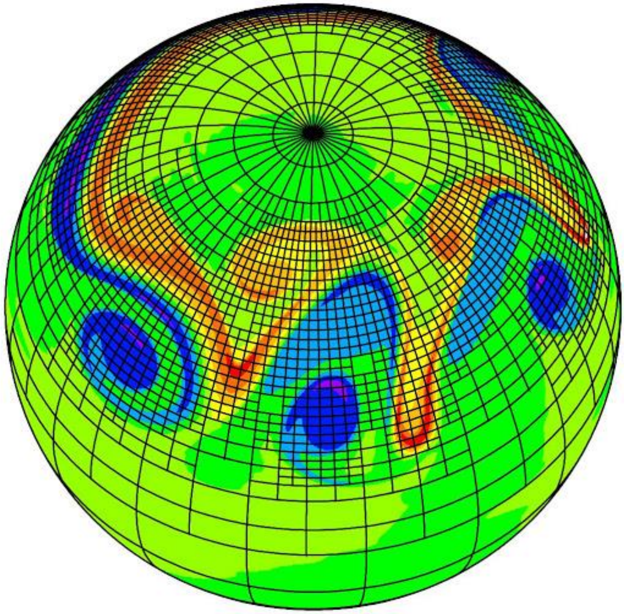

Cooling Rate at t=0

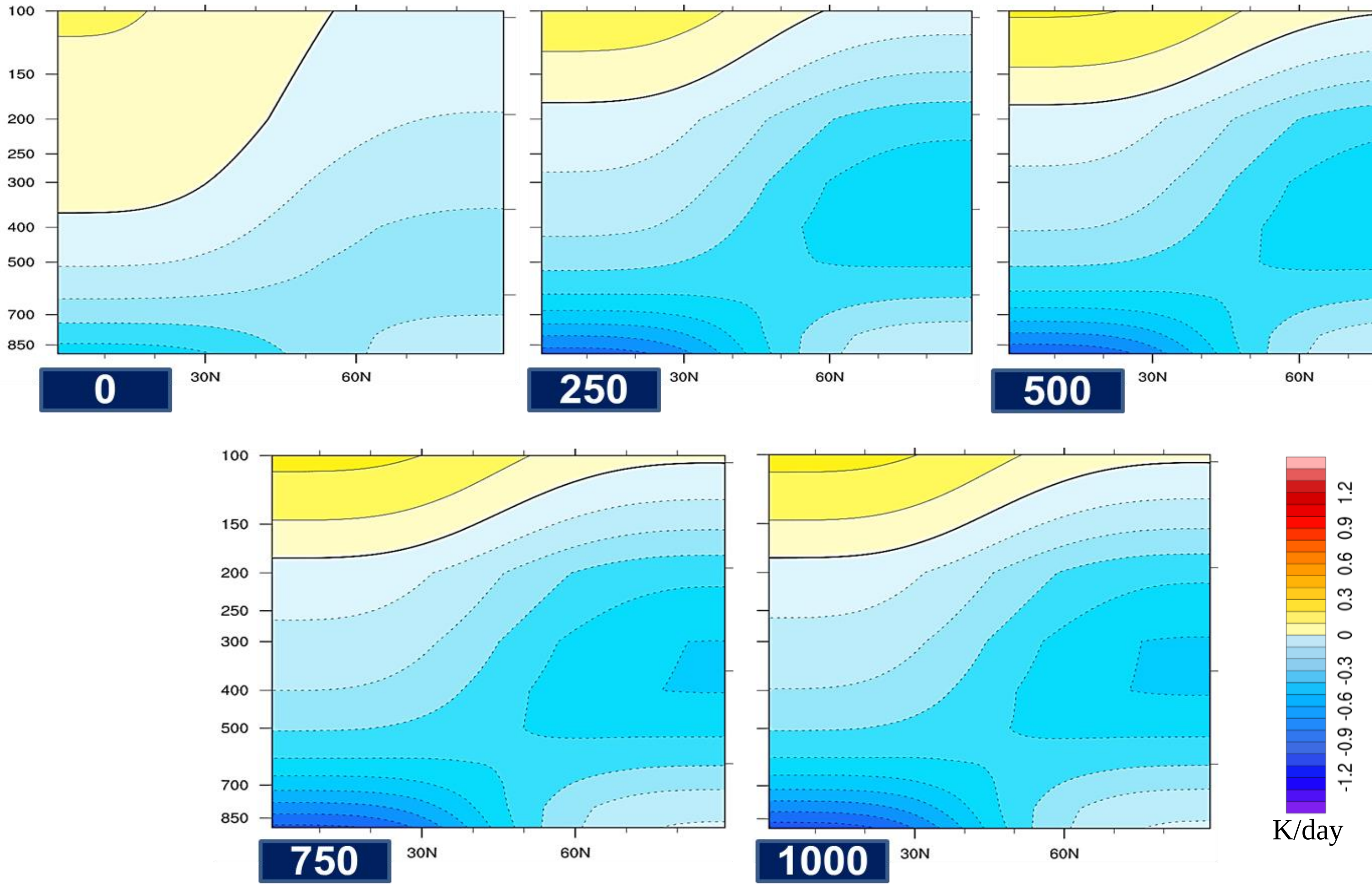

The contribution of CO_2 to net radiative heating is rather small in the troposphere, because the emitted radiation is reabsorbed at nearby levels with the same temperature. There is only a net radiative heating at the tropopause, where the temperature profile has a minimum value. It is also interesting to note that the CO2 radiative impacts on baroclinic instability are saturated at 750 ppm.

Eddy Activity & CO_2 Radiative Effects

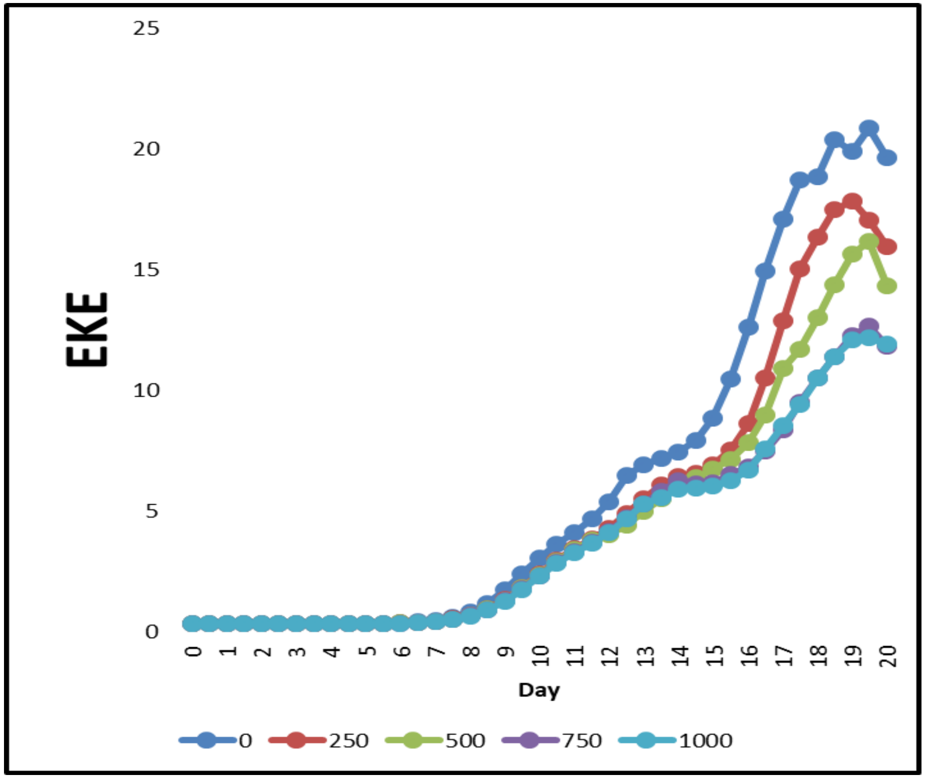

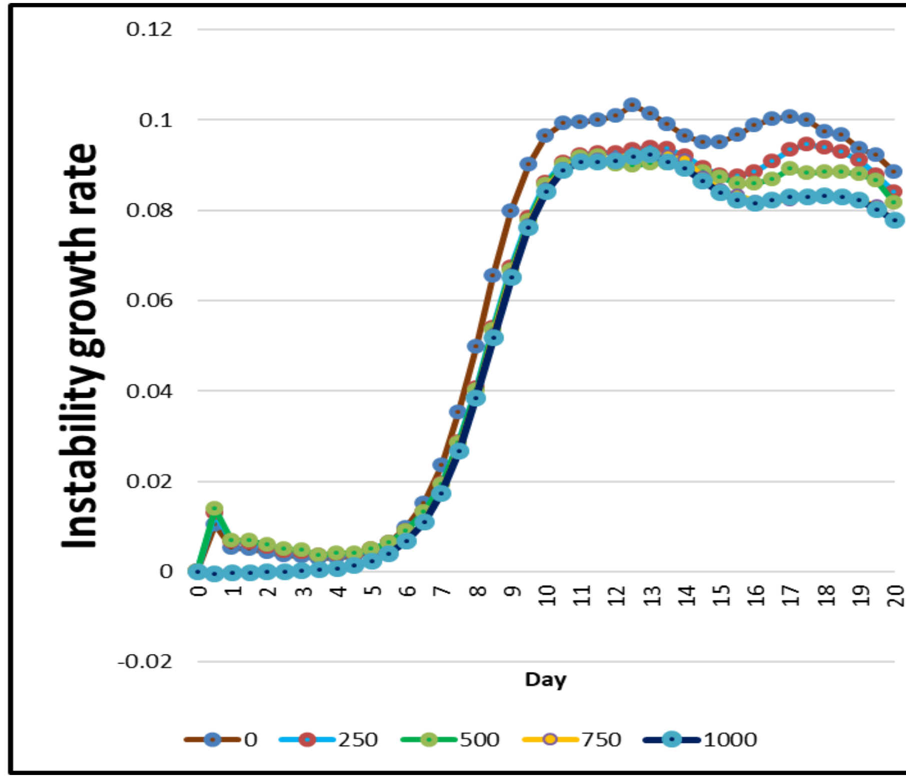

$$EKE = \frac{1}{2}(u'^2 + v'^2)^{1/2}$$

$$\sigma = \frac{\log(K'_t / K'_0)}{t}$$

For all experiments baroclinic instability forms at t=9 and eddy's decay (barotropic phase) begins at t=20 by decreasing EKE and the falling growth rate. The values of EKE and sigma decrease with increasing of CO_2 concentrations. In addition, the different slope of diagrams show how eddies are formed and propagated for different amounts of CO_2. So baroclinic instability can be divided into five periods t:0-9, t:9-12, t:12-16, t:16-18 and t:18-20.

Potential Temprature Gradient at t=9

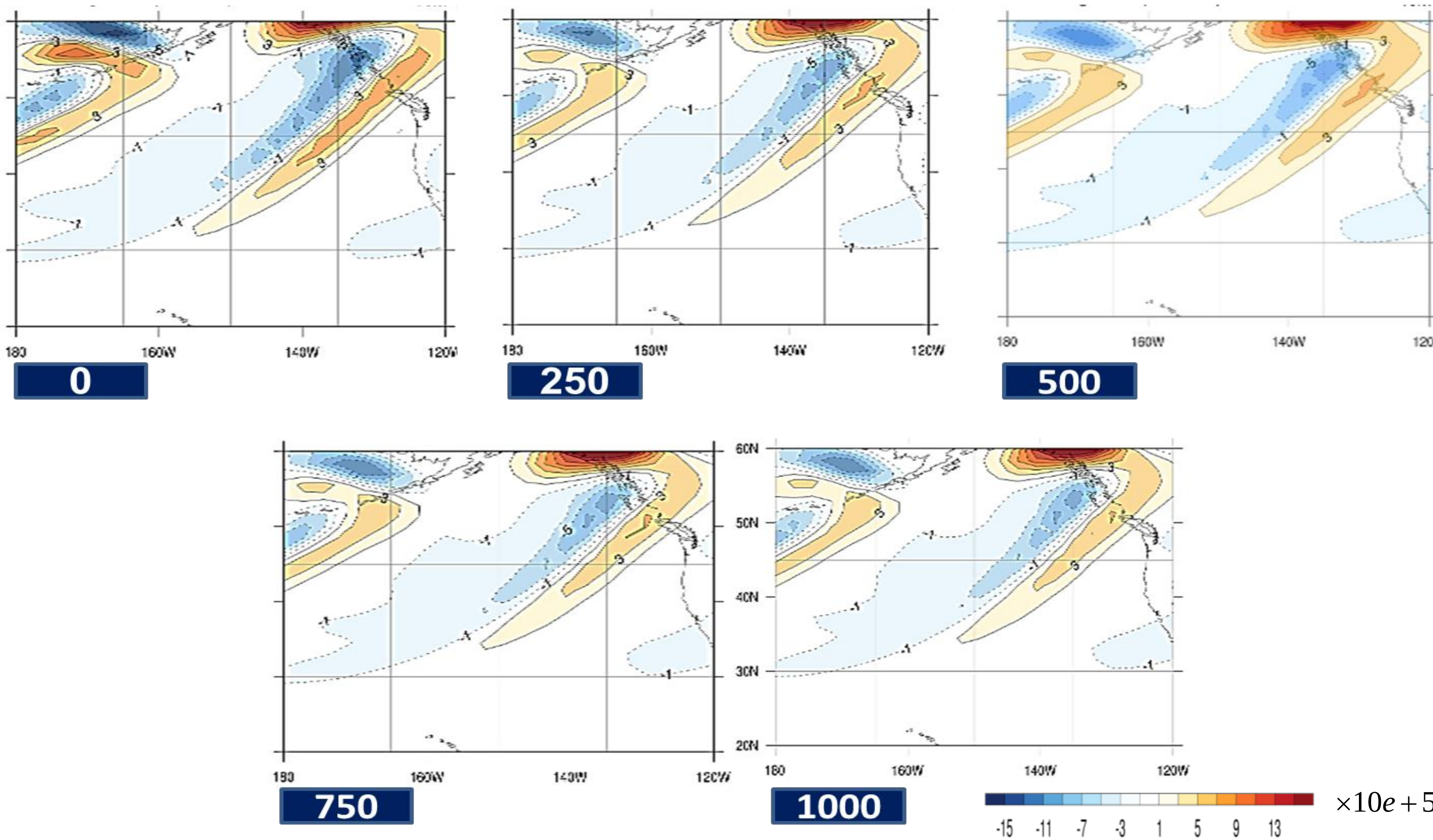

Eddy kinetic energy is derived from the eddy available potential energy, which is dependent on the mean available potential energy. Since the meridional temperature gradient is proportional to the mean available potential energy, it can affect eddy kinetic energy indirectly. The panels indicate the CO_2 radiative impacts on the meridional potential temperature gradient from 0 to 90N latitude and from 120W to 180W longitude at the 850 level. As expected, the meridional potential temperature gradient is reduced by increasing CO_2 concentrations through cooling in the lower latitudes at this level.

Cooling Rate Difference at t=0

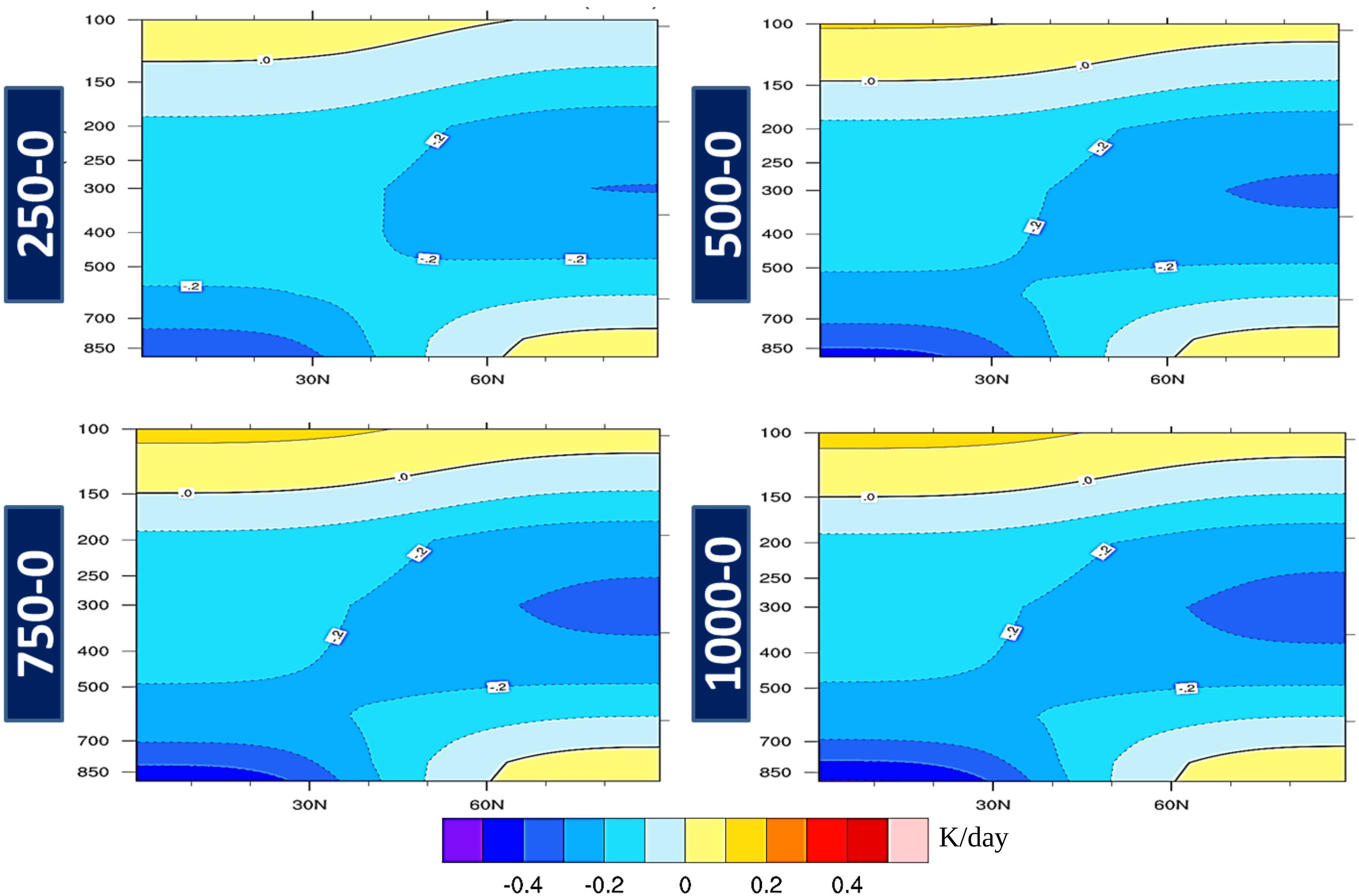

The baroclinic instability has not yet started at t=0, so the differences among the panels are due to increase in the atmospheric optical depth, through which the lower (upper) levels of the troposphere become colder (warmer) by increase in CO_2 concentration.

Cooling Rate Difference at t=9

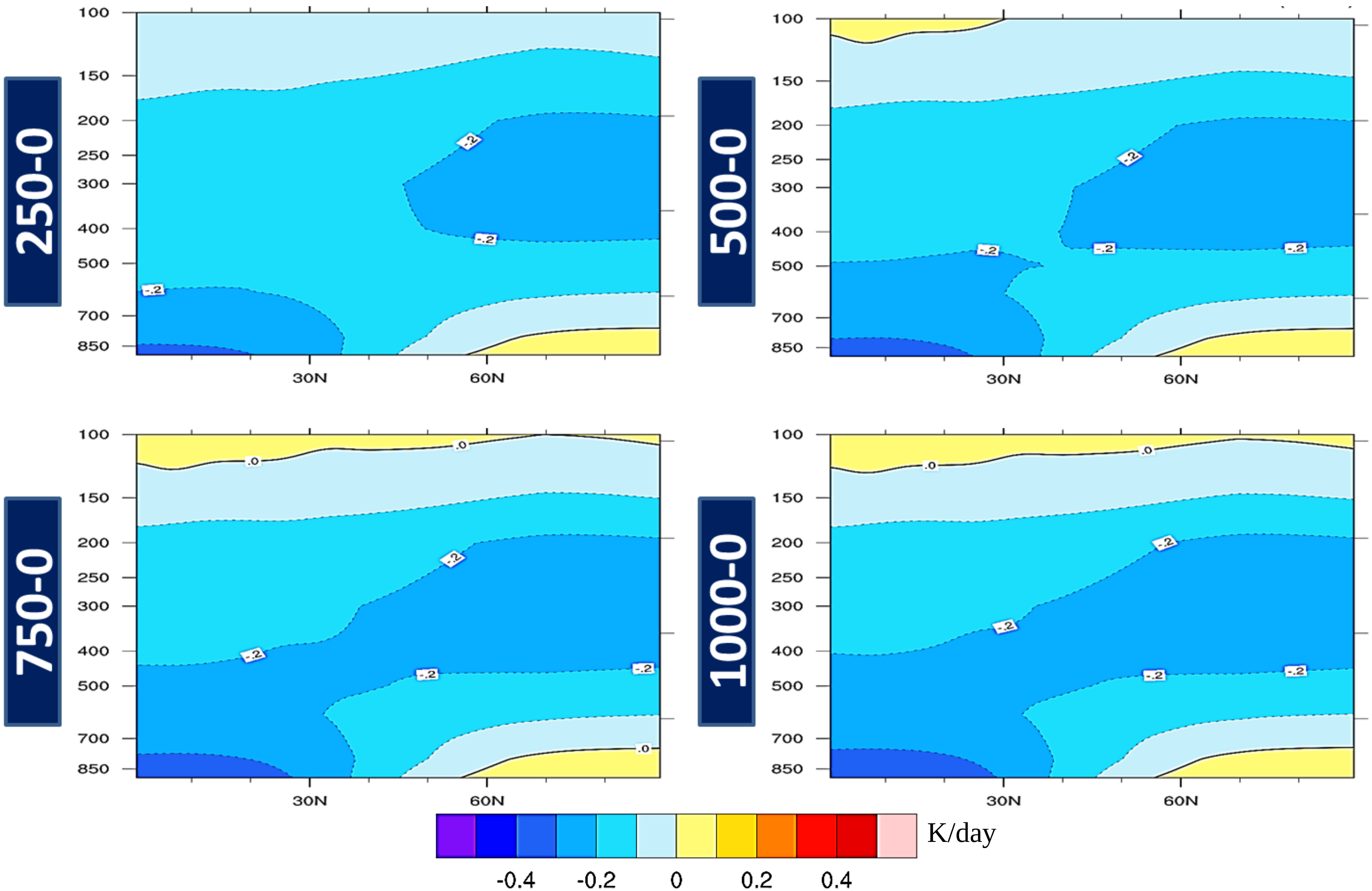

Since the interaction between radiation and the dynamical core is a two way relationship, large eddies relax the atmosphere to the initial state by meridional and vertical heat fluxes at t=9 (as instability forms). The polar heat flux changes the temperature field trough which affects radiative cooling rate. The reduction of radiative impacts is seen at t=9 compared to t=0 is seen in all the five experiments.

Cooling Rate Difference at t=18

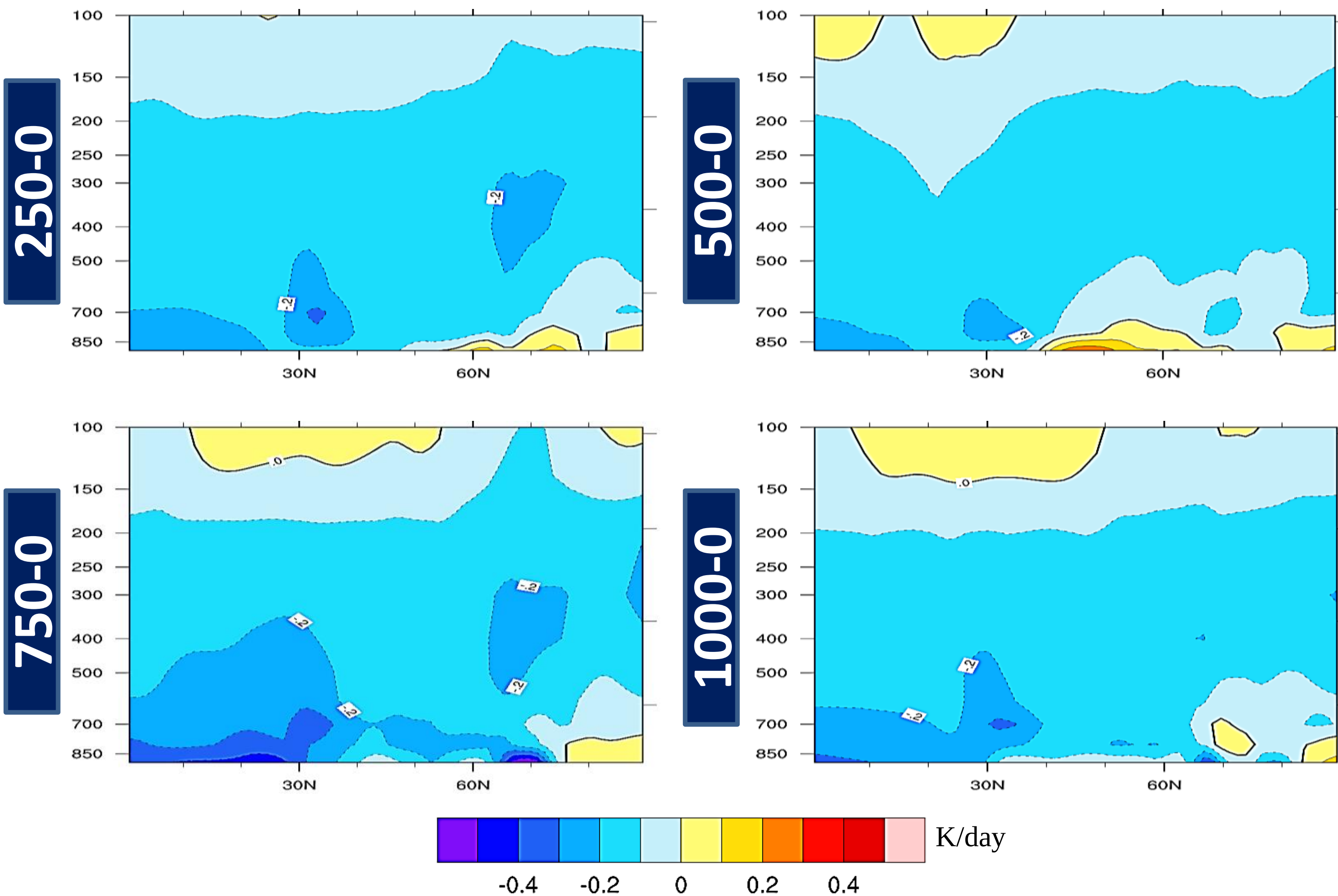

In the following days, eddy activities influence the temperature field which changes the cooling rate through thermodynamic energy equation.

Eddy-Mean Flow Interaction

Eliassen–Palm flux (Edmon et al, 1980)

$$F = \{F_y, F_p\} \quad ; F_y = -\overline{u'v'} \, , \, F_p = f \, \frac{\overline{v'\theta'}}{\overline{\partial\theta/\partial p}}$$

F_y → Meridional momentum flux → $KE \rightarrow KZ$

F_p → Meridional temprature flux → $AZ \rightarrow AE$

Eliassen–Palm flux divergence

$$\nabla \cdot F = \overline{v'q'} = \frac{\partial}{\partial y}(-\overline{v'u'}) + \frac{\partial}{\partial p}\left(f \, \frac{\overline{v'\theta'}}{\overline{\partial\theta/\partial p}}\right)$$

$\nabla \cdot F > 0$ → Source → Acceleration

$\nabla \cdot F < 0$ → Sink → Deceleration

Eddy-Mean Flow Interaction at t=9

Zonal mean zonal wind at the 200 hPa level; Jet : red solid line, EP flux : black arrow, EP flux divergence: shaded

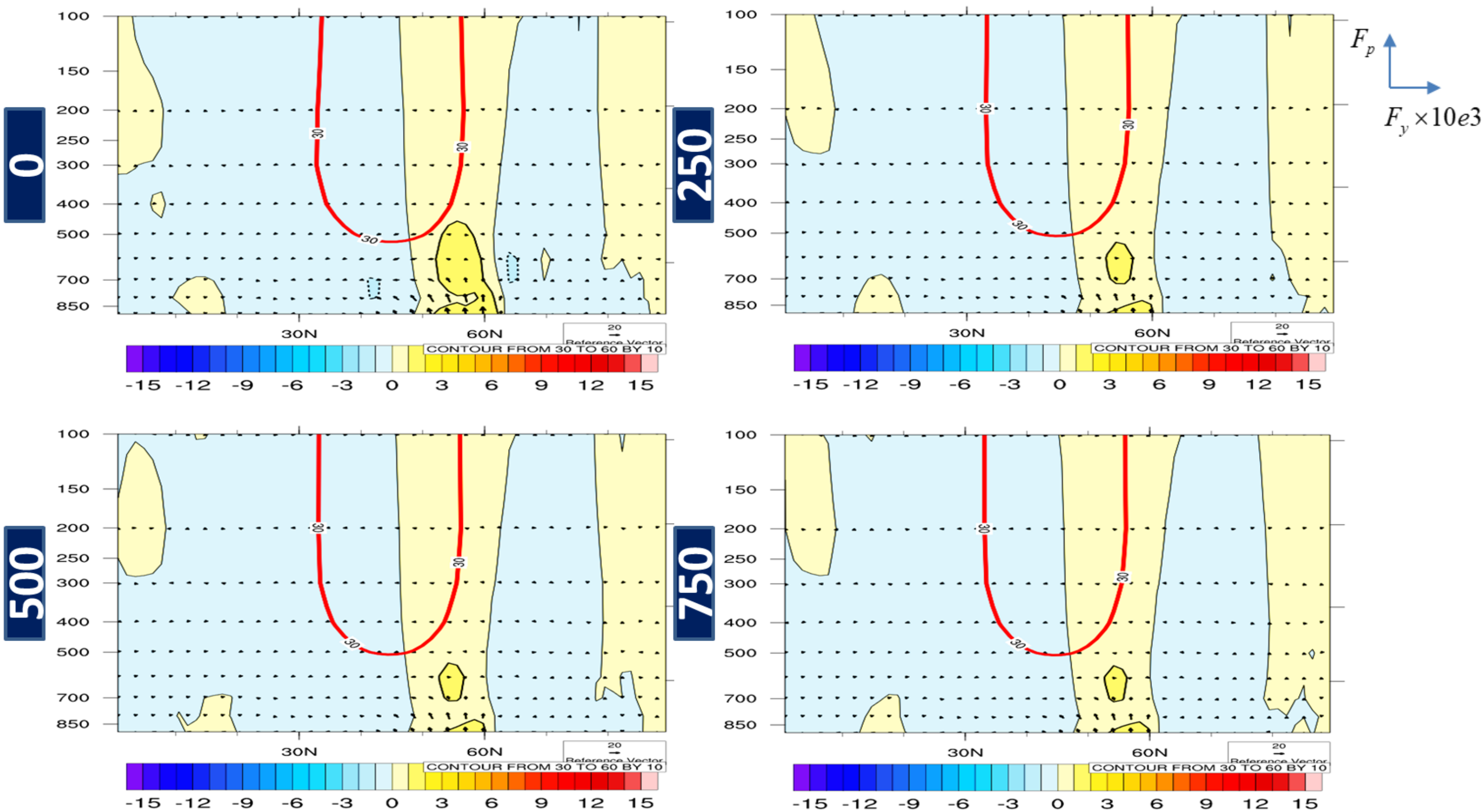

The divergence (convergence) zone is proportional to the energy source (sink) region, which is attenuated by increase in CO_2 concentration. As baroclinic instability forms (t=9), eddy activity is saturated at the lower troposphere. Furthermore, the CO_2 radiative impacts weaken the upward EP flux (proportional to the poleward heat flux, centered at latitude 50N) and subsequently the eddy's growth at lower levels.

Eddy-Mean Flow Interaction at t=12

Zonal mean zonal wind at the 200 hPa level; Jet : red solid line, EP flux : black arrow, EP flux divergence: shaded

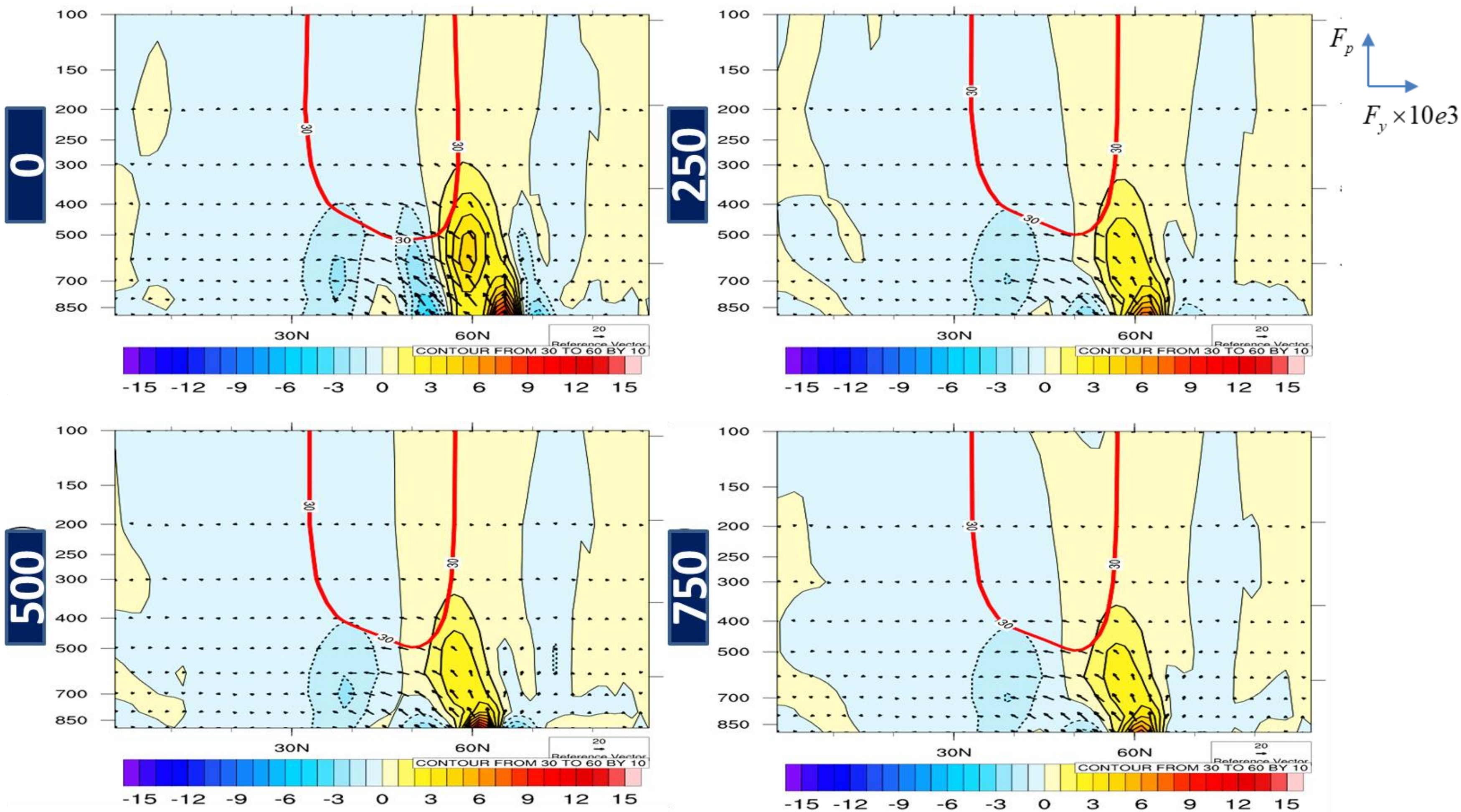

The wave packets propagate in meridional direction by forming the divergence and convergence zones sequentially. This propagation is directly related to the slope of EKE diagrams at all the five experiments. In the first experiment, the meridional propagation of waves occur with a higher energy level. In the other words, the consecutive areas of source and sink provide the growth of eddies more rapidly.

Eddy-Mean Flow Interaction at t=16

Zonal mean zonal wind at the 200 hPa level; Jet : red solid line, EP flux : black arrow, EP flux divergence: shaded

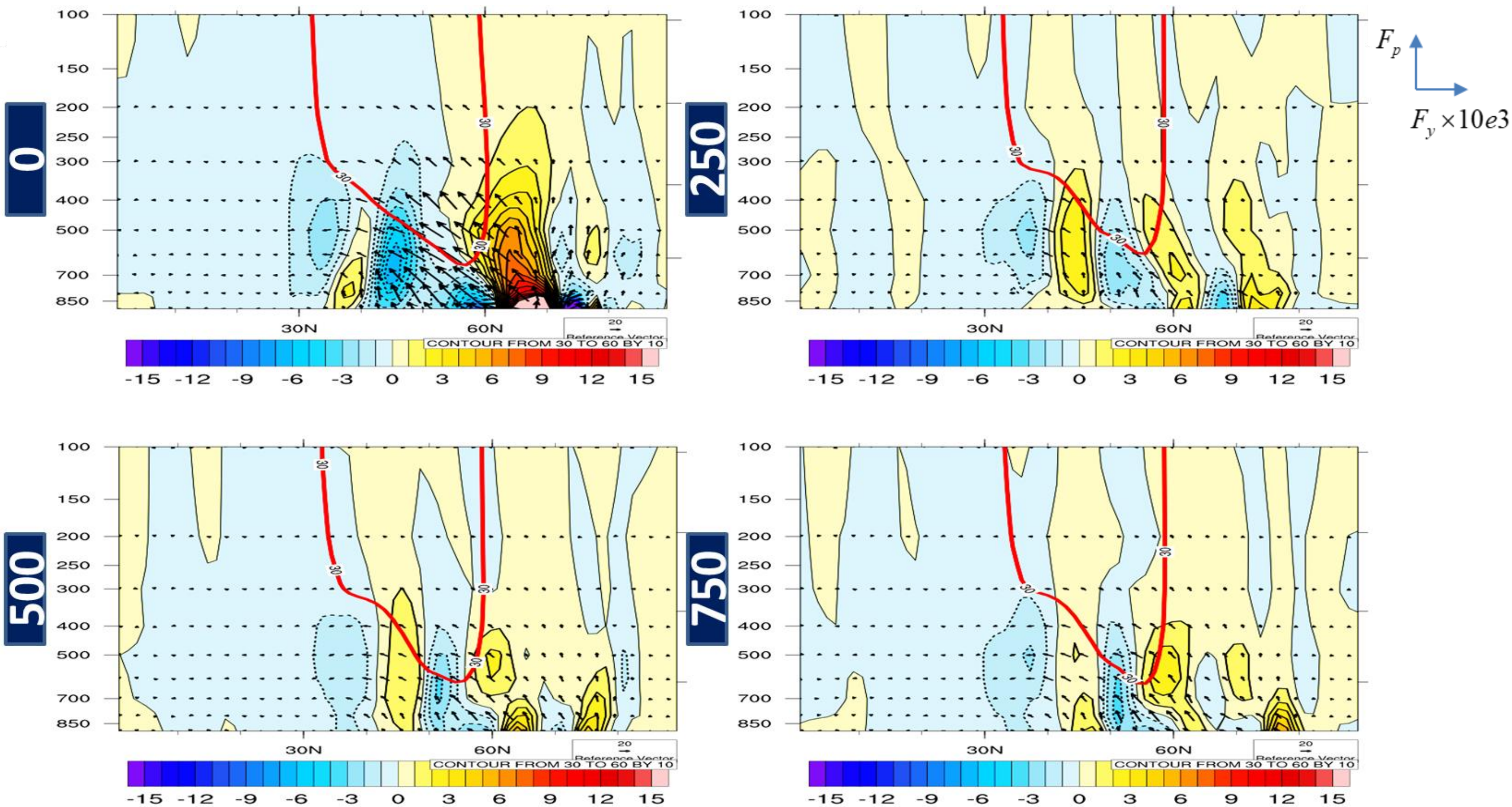

At this stage, the vertical extension of divergence (convergence) zones to the middle levels of the atmosphere affects the acceleration of wind (deceleration) and the upper-level jet. As this process continues, the jet becomes stronger (weaker) according to divergence (convergence) zones. For increasing CO_2 concentration and attenuation of the divergence zones, the meridional and vertical propagation of eddies are decreased at the lower levels, thereby weakening the jet.

Eddy-Mean Flow Interaction at t=18

Zonal mean zonal wind at the 200 hPa level; Jet : red solid line, EP flux : black arrow, EP flux divergence: shaded

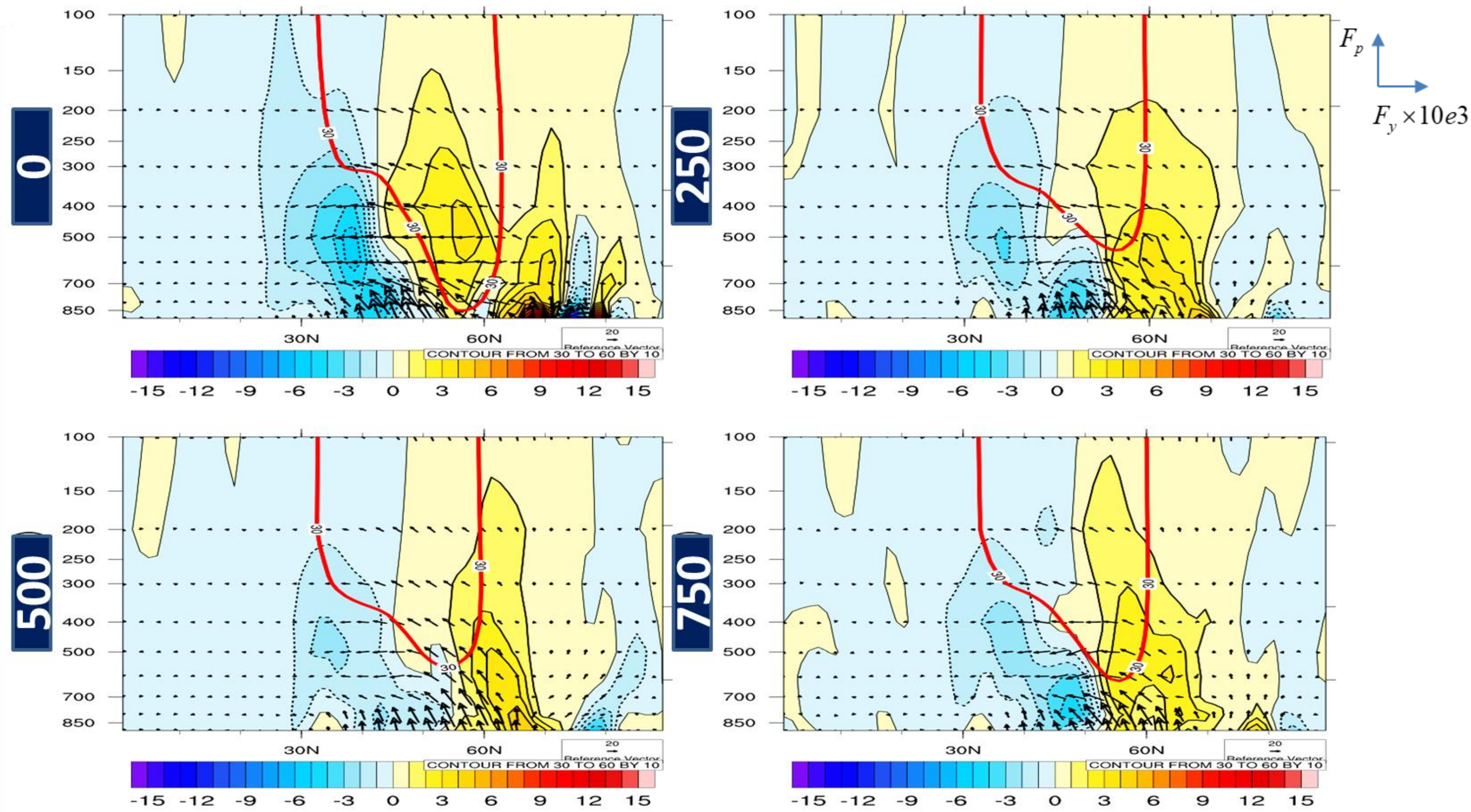

As the EP flux vectors become equatorward (proportional to the momentum fluxes), acceleration increases at the lower levels. So the eddy activity is saturated in the upper troposphere and the decay phase starts. This stage is proportional to the downward slop of the growth rate diagram.

Eddy-Mean Flow Interaction at t=20

Zonal mean zonal wind at the 200 hPa level; Jet : red solid line, EP flux : black arrow, EP flux divergence: shaded

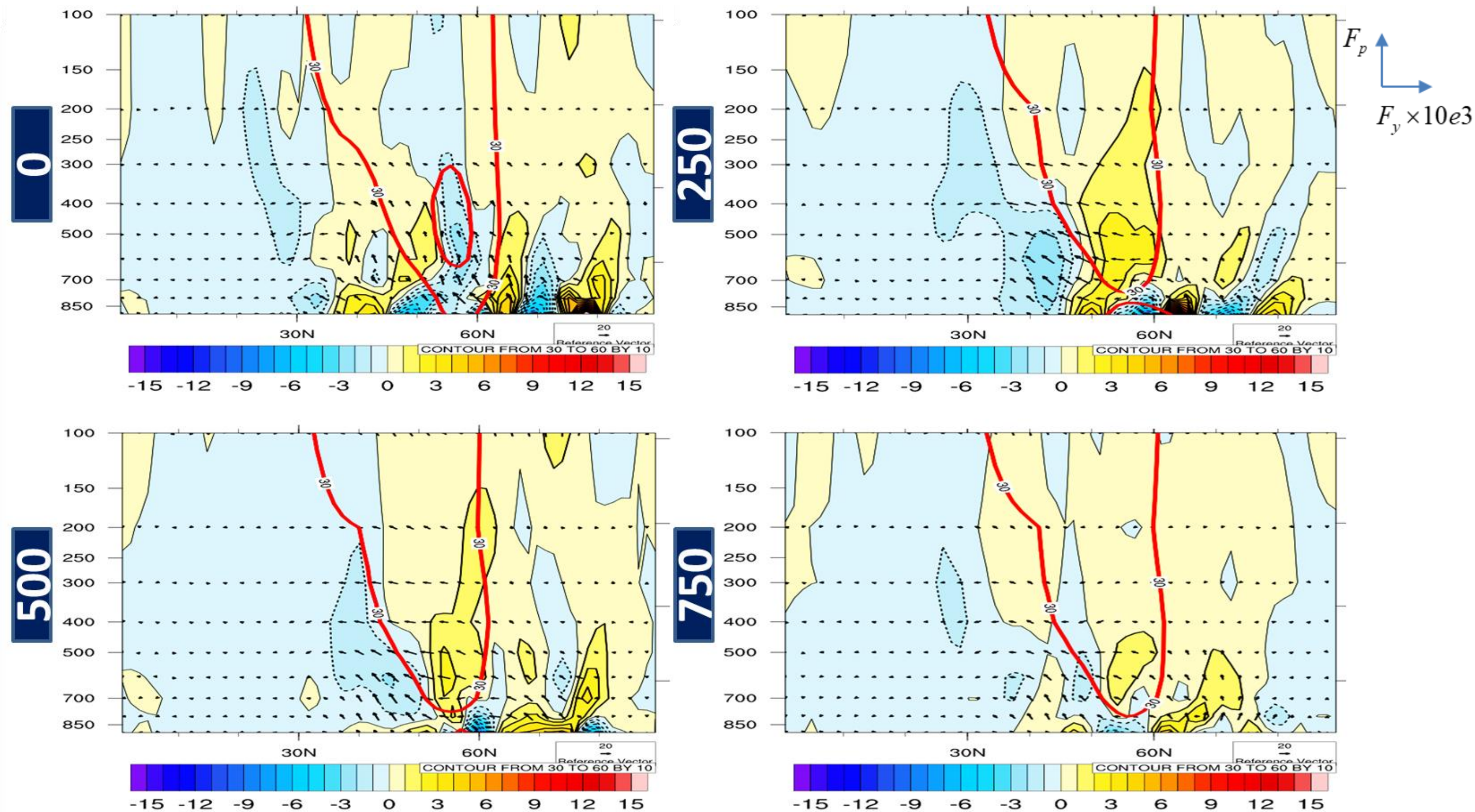

Proportional to the primary energy in each experiment (for different CO_2 concentrations), the atmospheric structure changes from baroclinic to barotropic by the conversion of eddy kinetic energy to mean kinetic energy at t=20.

Quantitative assessment

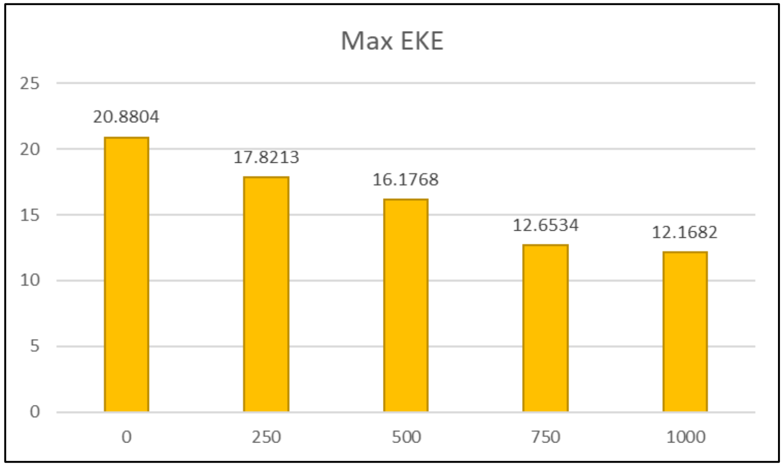

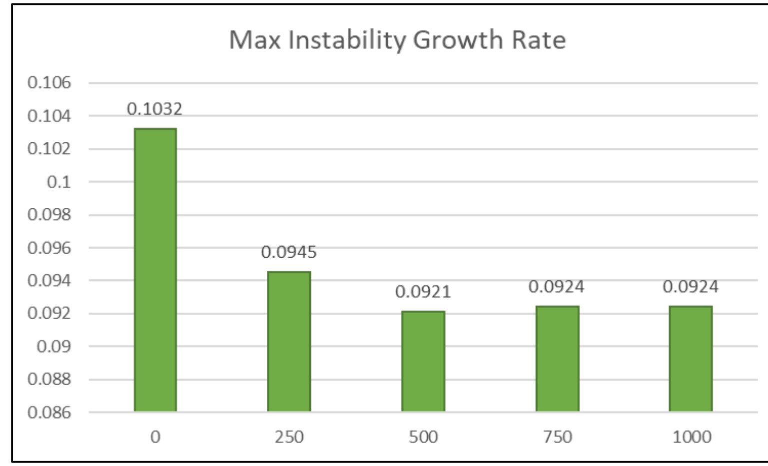

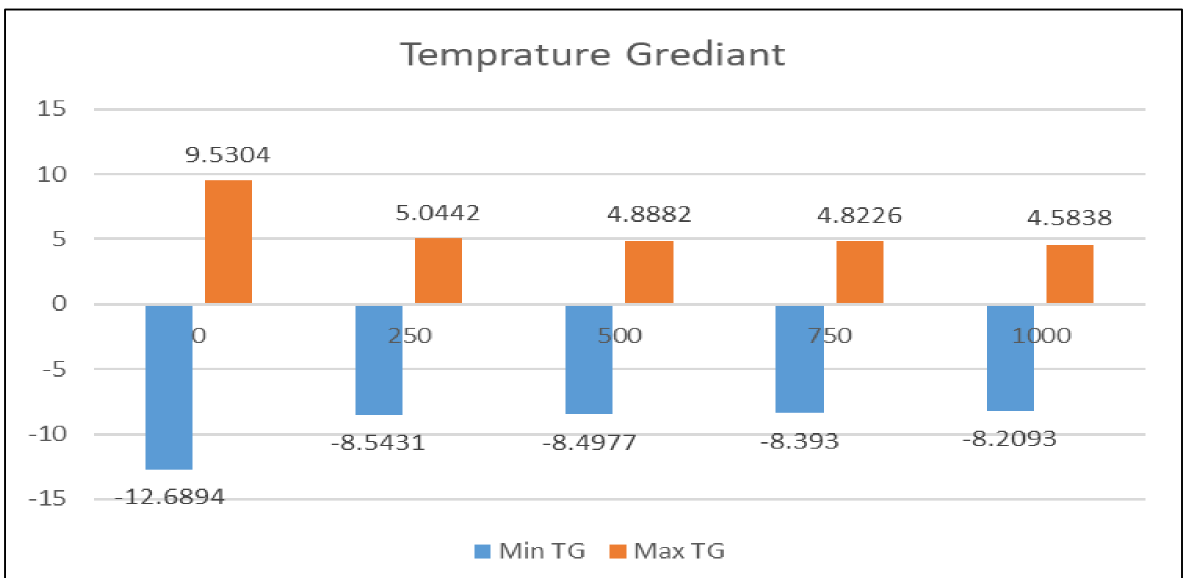

Quantitative assessment

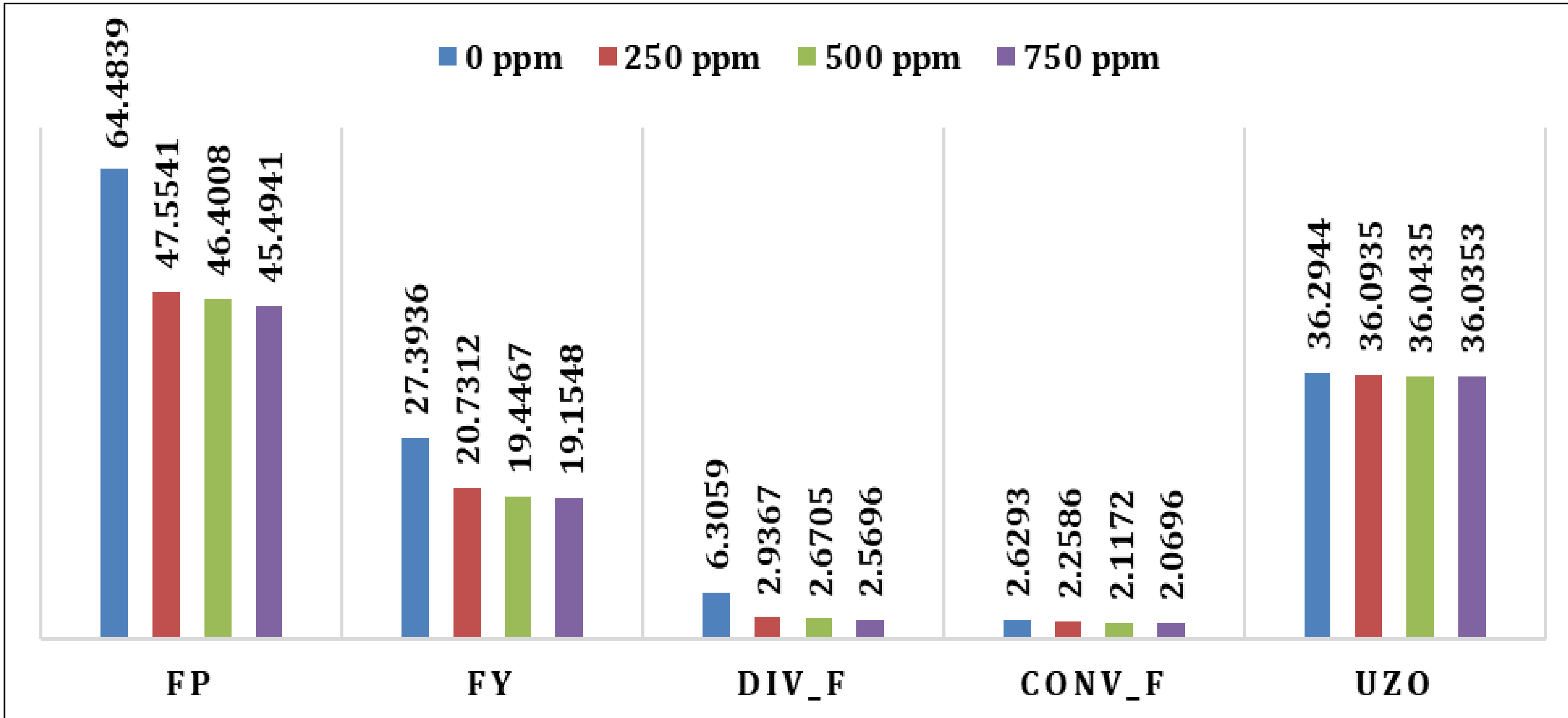

Maximum zonal-time average of upward (FP) and equatorward (FY) components of the EP flux, divergence (DIV_F) and convergence (CONV_F) of the EP flux and the jet (UZO)

Results

- Increase in the concentration of CO_2 decreases the meridional temperature gradient and thus reduces the eddy kinetic energy at lower atmospheric levels.
- Increase in the CO_2 concentration causes the growth rate, meridional and vertical eddy propagation and upper-level jet to weaken.
- The CO_2 radiative impacts on baroclinic instability are saturated at 750 ppm.

References

- Edmon, H. J., B. J., Hoskins, M. E., McIntyre, 1980: Eliassen-Palm Cross Sections for the Troposphere, *J. Atm. Sci*., **37**, 2600-2616.
- Jablonowski, C., and D. L. Williamson, 2006a: A baroclinic wave test case for dynamical cores of general circulation models: Model intercomparisons. NCAR/TN–469+STR, 75 pp.
- Jablonowski, C. D., and D. L. Williamson, 2006b: A baroclinic instability test case for atmospheric model dynamical cores. *Q. J. R. Meteorol. Soc*., **132**, 2943–2975.
- Mohebalhojeh, A. R., and D. G., Dritschel, 2004: Contour-advective semi-Lagrangian algorithms for many-layer primitive-equation models, *Q. J. R*. Meteorol. Soc., 130, 347–364.
- Mohebalhojeh, A. R., and D. G., Dritschel, 2007: Assessing the Numerical Accuracy of Complex Spherical Shallow-Water Flows, *Mon. Wea. Rev*., **135**, 3876-3894.
- Mohebalhojeh, A. R., and D. G., Dritschel, 2009: On the spectral convergence of the supercompact finite-difference schemes for the f-plane shallow-water equations, *Mon. Wea. Rev*., **137**, 2393-2406.
- Mohebalhojeh, A. R., M. Joghataei, D. Dritschel, 2016: Toward a PV-based algorithm for the dynamical core of hydrostatic global models. *Mon. Wea. Rev.,* **144**, 2481–2502.
- Petty, G.W., 2006*: A First Course in Atmospheric Radiation*, Sundog Publishing, 459 pp.